R4-C.2: Algorithms and Architectures for X-ray Diffraction Imaging

I. PARTICIPANTS

Faculty/Staff			
Name	**Title**	**Institution**	**Email**
David Castañón	PI	BU	dac@bu.edu
Clem Karl	Professor	BU	wckarl@bu.edu
Graduate, Undergraduate and REU Students			
Name	**Degree Pursued**	**Institution**	**Month/Year of Graduation**
Parisa Babahedarian	PhD	BU	12/2017

II. PROJECT DESCRIPTION

A. Project Overview

This project investigates the development of improved automated explosives detection and classification algorithms through the fusion of multiple modalities. Of particular interest are techniques that can potentially penetrate luggage and complement the information provided by dual-energy X-ray imaging. Our effort is focused on extracting additional signatures from X-ray excitation beyond the conventional density and effective atomic number by using X-ray diffraction.

The research accomplished several goals:

- Explored the benefits and implications of alternative architectures for X-ray diffraction imaging, including variation in source-detector configurations, types of detectors, and changes in source content.
- Developed and evaluated a suite of reconstruction algorithms for each architecture, and identified processing requirements as well as relative performance of the different algorithms in each architecture.
- Explored the need for fusion with dual energy CT reconstruction for different architectures to obtain reasonable performance.
- Explored new algorithm concepts based on compressive sensing to reduce computation and highlight structures in X-ray diffraction imaging.
- The majority of the results were documented in the Ph. D. thesis of Dr. Ke Chen [16] and the papers [16,17].

B. Biennial Review Results and Related Actions to Address

The majority of this project was completed by Year 2, and the project was expected to be terminated then. The effort in Year 3 was minimal; to educate a new graduate student to transition the methodology to other tasks. Hence, this project was not reviewed, and no actions were needed to address any deficiencies.

C. State of the Art and Technical Approach

X-ray Computed Tomography (CT) is a well-established modality for non-invasive medical diagnostic im-

aging and security inspection. In conventional single-energy transmission X-ray CT, an X-ray source with a given energy spectrum is used to radiate an object. The transmitted X-ray intensity through a straight-line path is measured at the detectors and used to construct estimates of the spatial distribution of the linear attenuation coefficient (LAC) of the material inside the object. In dual-energy systems, two different source spectra are used and the LAC is often represented in terms of two basis functions, corresponding to the Compton and photoelectric effects. For material identification purposes, the coefficients of these two basis functions are often transformed into estimates of density and an effective atomic number.

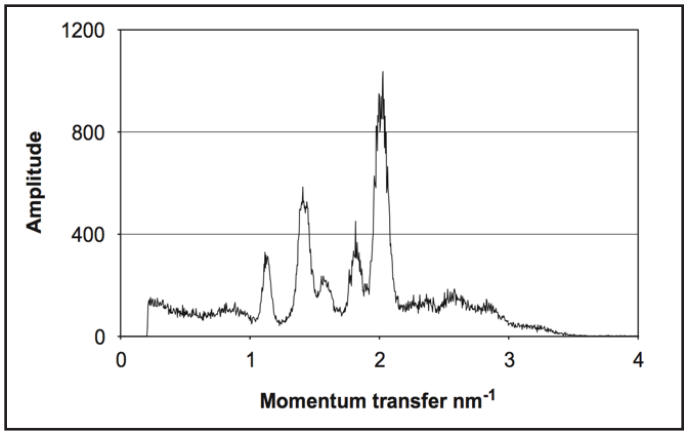

Figure 1: Coherent scatter form factor for TNT.

X-ray diffraction imaging (XDI) is currently an emerging technology that synthesizes two important characteristics of X-rays: their ability to form images and the ability to perform material analysis via representative X-ray diffraction profiles [8, 11, 12 and 18]. Originally developed as an analytical technique primarily used for the identification of crystalline material samples, XDI has been developed over the years to become an alternative imaging modality for performing spectroscopic analysis of complex, extended objects. In contrast to conventional X-ray imaging systems, XDI measures low-angle coherent scatter and yields the spatially resolved coherent-scatter form factor, also termed diffraction profile, illustrated in Figure 1. Locations of peaks in the diffraction profile, known as the Bragg peaks, provide molecular structure information that can be used as spectral signatures. The high dimensional nature of these feature profiles makes them desirable for distinguishing and detecting the presence of specific materials of interest.

XDI systems designed by Morpho Technologies have been incorporated into certified luggage inspection systems [5, 9 and 10]. However, these systems require the use of tube collimators that restrict observed scatter to a fixed scatter angle, in order to localize scattering location. They also require the use of polychromatic X-ray sources and narrow band photon-counting detectors to measure the diffraction profile at each detector given scattering at a specified angle. As a consequence, these systems have slow scan performance and low SNR for estimating the diffraction profile, as most of the scattered photons are at angles blocked by the collimators.

Alternative approaches based on X-ray Diffraction Tomography (XDT) have been proposed [11-14], whereby each detector can collect coherent scatter at multiple angles. These approaches combine X-ray CT and XDI techniques and, thus, use advanced reconstruction algorithms to localize the scattered radiation and estimate coherent scatter form factors for different spatial locations. Early reconstruction algorithms for XDT [13 and 14] were mostly based on algebraic reconstruction technique (ART) with high computational cost and exploited a dense angular imaging architecture similar to CT. A modified three-dimensional (3D) filtered back-projection (FBP) algorithm was developed in [15] that resulted with two orders of magnitude faster reconstruction speed compared to ART, although at a loss in reconstructed image quality and requiring dense spatial sampling. The algorithm also required monochromatic illumination; significant extensions would be required for using multi-energy illumination.

There has been extensive recent work at Duke University [18-24] on alternative X-ray diffraction architectures that use both multi-energy illumination and energy sensitive detectors, exploiting the use of coded apertures and advanced computational imaging algorithms to reconstruct the coherent scatter form factors. Most of their experiments to date focused on imaging isolated materials and have not addressed many of the concerns that arise when imaging luggage, such as the presence of significant attenuation, beam hardening, and interference from neighboring objects.

Motivated by these gaps in the available theory, we focused our efforts on studying tomographic imaging architectures for X-ray diffraction and corresponding computational inverse algorithms that were designed to work with multi-energy illumination for the imaging of densely packed volumes that include both metallic and non-metallic objects. Since these architectures were notional, most of our experiments involve detailed Monte Carlo simulations of measurements provided by simulators such as GEANT4 [25] and are, thus, limited in scope due both to computational limitations as well as the difficulty in mathematical representation of the contents of suitcases. In our work [16 and 17], we developed novel tomographic inversion techniques that lead to enhanced image formation and material identification, and improved upon the reconstruction algorithms provided by ART. By extension of our previous work on THz diffraction tomography, we studied alternative architectures for imaging densely packed diverse materials and identified relative strengths and weaknesses for use in future luggage inspection systems. We discuss the foundations of X-ray diffraction and our technical approach below.

The interaction of X-ray photons with matter in an energy range between 20 and 150keV can be described by photoelectric absorption and scattering. Scattering encountered in radiology arises through coherent (Rayleigh, elastic) scattering and Compton (inelastic, incoherent) scattering. Whereas Compton scattering varies slowly with angle, coherent scatter occurs mostly in forward directions and its angular spread has a distinct structure, characteristic of the type of material. Coherent scatter is often measured in terms of a scattering form factor $|F(q)|^2$, where q is the momentum transfer and the form factor is proportional to the scattering cross-section of the material. The momentum transfer parameter q depends on the excitation wavelength λ and the deviation angle Θ from the straight path, as:

$$q = \frac{1}{\lambda}\sin(\frac{\theta}{2}),$$

Hence, there are different ways to vary and measure momentum transfer. For example, knowing the X-ray excitation energy, and observing the scattered photons at different angles will vary q. Alternatively, knowing the angle of observation varying the excitation energy (thus wavelength), will vary q. The latter approach is used in current commercial scanners [9 and 10], where the deviation of broad spectrum X-rays are measured at a single fixed deflection angle, as constrained by tube collimators, and photon-counting detectors can measure the relative photon counts for the different energy levels, corresponding to different momentum transfer levels. Such an architecture is illustrated in Figure 2 and has the advantage that the material in question is interrogated from a single direction, rather than requiring multiple directions. In addition, each detector is focused on a unique voxel, making the association between the measured scattering form factor and the physical location straightforward. However, the main limitation of the architecture is that most of the scattered photons fail to reach the detectors and, hence, it takes significant time to acquire sufficient signal strength to discriminate materials reliably.

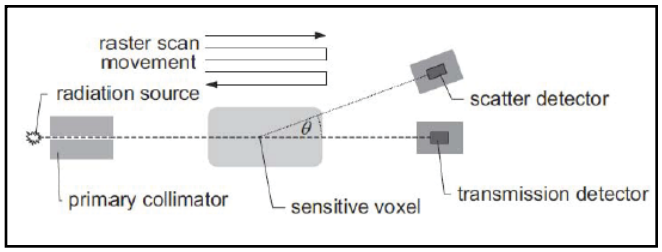

Figure 2: X-ray diffraction imaging system.

In our work, we focused on two alternative architectures that show promise for increasing signal strength by collecting scattered photons from multiple locations at each detector. This implies that the localization of scattered photons must be done computationally through the solution of an inverse problem. The first architecture is an XDT architecture similar to that proposed in [12] and shown in Figure 3. In this architecture, a given plane in an object is illuminated and off-plane detectors collect scattered information from multiple locations in the plane. The illumination source rotates around the object, along with the detectors, providing multiple views of the object. In order to isolate the number of locations that contribute to scatter in each

off-plane detector, vertical collimators are used to restrict the locations that contribute scattered photons to a detector to those locations in a beam aligned with the projection of the detector on the illuminated plane. In such an architecture, the source and detectors would rotate as in current CT systems. Alternative versions of this architecture that would not rotate detectors include electron-beam tomography, but the source would be excited from different locations. While our analysis focused on the rotating architecture, the results would be similar when using architectures such as electron-beam tomography.

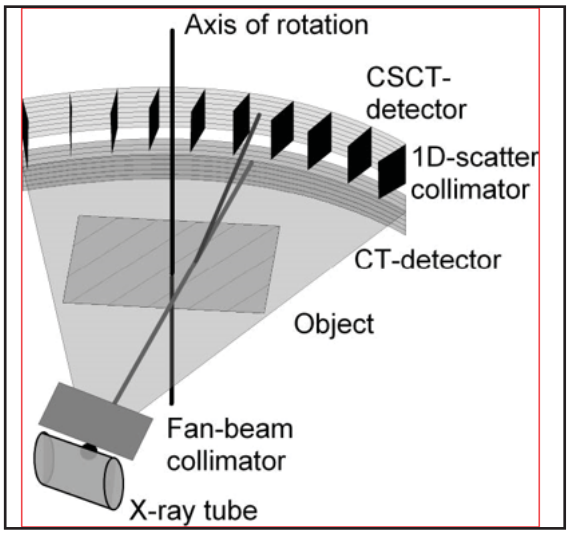

Figure 3: Tomographic X-ray diffraction.

The second class of architectures we studied were coded aperture architectures, where the object of interest is not required to rotate between the source and detectors. This architecture is similar to that proposed in [19 and 20] and uses a coded aperture mask between the object of interest and the detectors, as illustrated in Figure 4. This architecture differs from the first architecture in several ways. First, it uses three fixed projections, as opposed to a rotating set of projections. Second, the system allows for the mixing of scatter signals from multiple beams in the plane, thereby collecting more of the scattered photons at the detectors.

The three directions of illumination are chosen to be 60 degrees in orientation to provide illumination diversity. Each direction illuminates a plane in the object and allows the scattered photons to scatter off-plane to a set of scatter detectors. Unlike the approach in Figure 3, no collimators are used between columns of detectors; instead, scattered photons from the entire plane pass through a coded aperture that blocks some scatter directions on the way to detectors. Figure 4 illustrates one direction of illumination, where a plane of X-ray excitation at wavelength λ illuminates the object under investigation. Coherent scatter radiation from the illuminated plane passes through a coded aperture before reaching a 2D detector array.

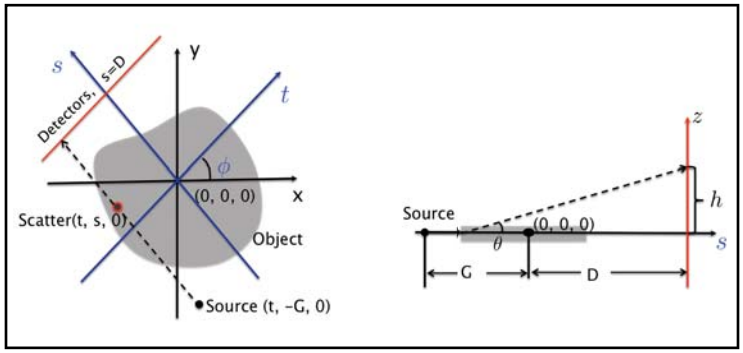

Figure 4: X-ray diffraction imaging.

We developed mathematical models of the above XDI systems and used them as the basis for developing tomographic reconstruction algorithms for X-ray diffraction images. The details of these algorithms are documented in our paper [18] and the thesis [1]. We provide a brief overview of the formulation and techniques below.

Consider the illumination geometry illustrated in Figure 4 without the code aperture. The object is being illuminated at a projection angle Φ by source G units away from the detector array. The intensity at wavelength λ at $(t, s, 0)$ is given by

$$I_\lambda(t,s) = I_\lambda \exp\left[-\int_{D-G}^{s} \mu_\lambda(t,s',0)\, ds'\right] \triangleq I_\lambda \mathcal{A}_\lambda(t,s,0)$$

where $A_\lambda(t,s,0)$ is the exponential expression describing the attenuation along with the incoming radiation that reaches the object at voxel $(t,s,0)$. The intensity of coherent scattering from a voxel centered at $(t,s,0)$

towards the detector element at position (*t, D, h*), where *h* is the off-plane height of the detector, can be modeled as

$$\tilde{I}_\lambda(t,s,D,h) = I_\lambda(t,s)|F(t,s,\frac{1}{\lambda}\sin(\frac{1}{2}\arctan(\frac{h}{D-s})))|^2 \approx I_\lambda(t,s)|F(t,s,\frac{h}{2\lambda(D-s)}))|^2,$$

except a constant factor describing the proportionality. The form factor of interest that we are trying to reconstruct is *F*(*t,s,*q) at each voxel position (*t,s*) for each momentum transfer level *q*. The last approximation assumes small scatter angles that are typical of coherent scatter.

In our rotating XDT systems, detector columns are separated by sheet collimators whose blades are angled towards the source. This guarantees that detector element at (*t, D, h*) only collects photons from scattering along the same *t*, mixed from different *s* positions. Let B_λ(*t, s, h*) be the wavelength-dependent attenuation from the coherent scatter at (*t, s, 0*) to the detector element at (*t, D, h*); the intensity received at this detector element is given by

$$I_\lambda(t,s,D,h) = \tilde{I}_\lambda(t,s,D,h)\mathcal{B}_\lambda(t,s,D,h)$$

For intensity detectors with cutoff frequencies (λ_{min}, λ_{max}) and area *A* at off-plane height *h* from the illumination plane, the effective area exposed to radiation is

$$\mathcal{E}(s,h) = \frac{A(D-s)}{(h^2+(D-s)^2)^{3/2}}.$$

and the overall intensity detected at (*t, D, h*) is the integration over the voxels along path at *t* inside the object, averaged over the intensity distribution over frequency, as

$$I_\phi(t,h) = \int_{\lambda_{min}}^{\lambda_{\max}} \int_{D-G}^{D} I_\lambda \mathcal{A}_\lambda(t,s,0)\mathcal{B}_\lambda(t,s,D,h)\mathcal{E}(s,h)|F(t,s,\frac{h}{2\lambda(D-s)})|^2 ds d\lambda$$

The above equation represents the basic mathematical model relating the observed measurements, highlighting a key issue: to model the measurements, one requires knowledge of the frequency dependent attenuation (*A*, *B* in the equation above) along the transmitted and scattered paths. That may require information collected from dual-energy or multi-energy transmission imaging.

The above measurement model was derived for energy detectors. If photon-counting detectors are used with frequency bins of half width *Δ* centered at frequencies λ_k, the observation model yields an energy in each bin, as

$$I_\phi(t,h,\lambda_k) = \int_{\lambda_k-\Delta}^{\lambda_k+\Delta} \int_{D-G}^{D} I_\lambda \mathcal{A}_\lambda(t,s,0)\mathcal{B}_\lambda(t,s,D,h)\mathcal{E}(s,h)|F(t,s,\frac{h}{2\lambda(D-s)})|^2 ds d\lambda$$

The above measurement model is based on restricting the scatter to a vertical off-plane direction. In our coded aperture architectures, we allow more general scatter directions, so this model gets modified to include effective cross-area for off-line detectors, as

$$\mathcal{E}(t,s,t',h) = \frac{A(D-s)}{\left((t'-t)^2+(D-s)^2+h^2\right)^{3/2}} \cdot T\left(t+\frac{D_c-s}{D-s}(t'-t)\right)$$

and the new measurement models depend on the side offset *t'* as well as the height *h*, given by

$$I_\phi(t',h,\lambda_i) = \int_t \int_s \int_{\lambda_i-\Delta}^{\lambda_i+\Delta} I_\lambda(t,0)\mathcal{A}_\lambda(t,0,s,0)\mathcal{B}_\lambda(t,s,t',h)|F(t,s,\frac{h}{2\lambda\sqrt{(t'-t)^2+(D-s)^2}})|^2\mathcal{E}(t,s,t',h) d\lambda ds dt$$

To construct the images from X-ray diffraction measurements in both systems above, we used computational imaging approaches that exploited the sparse measurement structure. The detailed approaches were documented in the thesis [26]. We pose the XDI reconstruction problem as an inverse problem, reconstructing objects slice by slice, estimating for each illuminated object slice a 3-dimensional intensity distribution *b* (in *x*, *y* and *q*) from its observations *y*. Here, the imaged field of view is discretized into *N* spatial *x, y* voxels, and at each voxel the field has an *M*-dimensional value, where *M* is the number of momentum transfer levels. Discretizing the measurement models discussed previously yields a model expressed as

$$\mathbf{y} = \mathcal{C}\mathbf{x} + \mathbf{n}, \qquad \mathbf{y} \in \mathbb{R}^{N_y},\ \mathbf{n} \in \mathbb{R}^{N_y},\ \mathbf{x} \in \mathbb{R}^{N_x}$$

where the variable n represents model errors. Below, we highlight two algorithmic approaches for constructing the images; the details of these and other approaches were documented in [26].

The first approach is based on using total variation regularization on the image derivatives. We used this regularization on the spatial coordinates but not on the momentum transfer coordinate because we expected to image objects with spatial extent, however, the coherent scatter form factors had different structure. Our algorithm IRL1 obtains the reconstruction by solving the optimization problem:

$$\min_{\mathbf{x}} \|\mathbf{y} - \mathcal{C}\mathbf{x}\|^2_{W_y} + \alpha^2 \|\mathcal{D}\mathbf{x}\|_1 \qquad \mathbf{x} \in \mathbb{R}^{N_x}_+$$

where W_y is a data-dependent diagonal matrix used to represent the Poisson nature of the measurements. We solve this nondifferentiable convex optimization problem using standard approaches such as half-quadratic approximations.

The second algorithm is based on edge-preserving regularization, explicitly attempting to estimate boundaries between spatial objects in an approach that generalizes the well-studied Mumford-Shah functional for image segmentation. Using the Ambrosio-Tortorelli relaxation, for each spatial voxel (*x,y*), we estimate a boundary field *s*(*x,y*) that can be interpreted as the probability that this voxel is an object boundary. Our algorithm IREP solves for the reconstructed image and the boundary field in an integrated optimization approach, with objective based on our previous work [1-4], as

$$\min_{(\mathbf{x},\mathbf{s})} \|\mathbf{y} - \mathcal{C}\mathbf{x}\|^2_{W_y} + \alpha^2 \|\mathcal{D}\mathbf{x}\|^2_{W_s} + \gamma^2 \|\mathcal{D}\mathbf{s}\|^2 + \frac{1}{\gamma^2}\|\mathbf{s}\|^2$$

where W_s is a diagonal weight matrix that avoids regularization near edges, as

$$W_s = \mathrm{Diag}\left[(1 - [\mathbf{s}]_i)^2\right]$$

To evaluate the performance of our algorithms, we used a couple of simple test phantoms that could be simulated for each of our architectures. One of these phantoms is a 3-dimensional block composed of a mixture of crystalline and amorphous materials: PVC, PMMA, Graphite, and Aluminum. The phantom is homogeneous in the vertical dimension; since coherent scatter is measured off the plane of illumination, the vertical dimension affects the coherent scatter through absorption of the scattered radiation, with significant reduction in signal strength. This phantom is illustrated in Figure 5 (on the next page) along with the momentum transfer form factors and the linear attenuation coefficients for each material. This phantom has materials with both concentrated form factors with sharp peaks (graphite, aluminum) as well as diffuse form factors (PMMA, PVC). It also has significant metal content with a high linear attenuation coefficient, which can lead to the creation of artifacts. Our main reasons for exploring this phantom was to determine the types of artifacts that result in the architectures for X-ray diffraction imaging and to identify algorithms that can mitigate those artifacts.

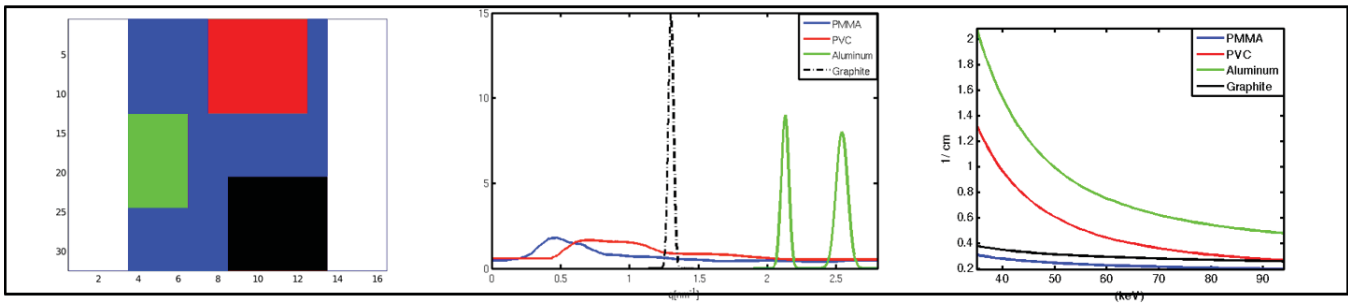

Figure 5: Left: Experiment phantom; Middle: momentum transfer form factors; and Right: linear attenuation coefficients for each material in the phantom.

One of the main results of our analysis was to evaluate whether one needed accurate information regarding the energy-dependent linear attenuation coefficients of the object of interest, which would have to be obtained from other modalities such as dual-energy imaging. Our measurement model above requires such knowledge to compensate for photon losses along the incoming and scattered path. Without this information, one must make approximations regarding these losses as part of the reconstruction algorithms. One possible approach to avoid this is based on our extensions of an approximation suggested in [15], as follows. The idea is to obtain a measurement of energy received along the transmission path and define new measurements based on the ratio of the scattered measurement energy to the transmitted measurement energy. For photons with energy level λ, the attenuation along the scattering path can be approximated by the attenuation along the transmitted path as:

$$\mathcal{B}_\lambda(t, s, D, h) \approx \mathcal{B}_\lambda(t, s, D, 0).$$

Then, we define the ratio measurement for the tomographic architecture with vertical collimation as

$$P_\phi(t, h, \lambda) \triangleq \frac{I_\phi(t, h, \lambda)}{I_\phi(t, 0, \lambda)} = \int_0^D \frac{(D-s)}{\left((D-s)^2 + h^2\right)^{3/2}} |F(t, s, \frac{h}{2\lambda(D-s)})|^2 ds$$

Note that, with the approximation, the normalization yields a model that no longer requires knowledge of the attenuation. However, this model requires monochromatic illumination as well as the approximation of the attenuation. If the X-ray source had a spectrum, even if measured using photon-counting detectors, the ratio would be:

$$P_\phi(t, h, \lambda_i) \triangleq \frac{I_\phi(t, h, \lambda_i)}{I_\phi(t, 0, \lambda_i)} \approx \frac{1}{2\Delta} \int_{\lambda_i - \Delta}^{\lambda_i + \Delta} \int_0^D \frac{\mathcal{E}(s, h)}{\mathcal{E}(0, 0)} |F(t, s, \frac{h}{2\lambda(D-s)})|^2 ds d\lambda$$

and the last simplification requires that straight path attenuation and intensity are approximately constant in the frequency range of interest.

To evaluate whether this approximation is sufficient, we performed reconstructions using both accurate linear attenuation coefficients as well as the approximations developed when one did not have this side information, using multi-energy excitation from 60 to 72 keV and photon counting detectors with 4 keV resolution, along with the X-ray diffraction architecture of Figure 3. The results are summarized in Figure 6 using the IRL algorithm. The IREP algorithm gives similar results. The results highlight that, for this architecture, the use of the approximate model provides reconstructions that are only slightly degraded relative to the reconstructions obtained using the side information when photon counting detectors are used, even with a coarse energy resolution. This suggests that the architecture of Figure 3 can form images without fusion from dual-energy CT when using photon-counting detectors. Other results we obtained indicate that this is not true when only using energy detectors and can be found in [17 and 26].

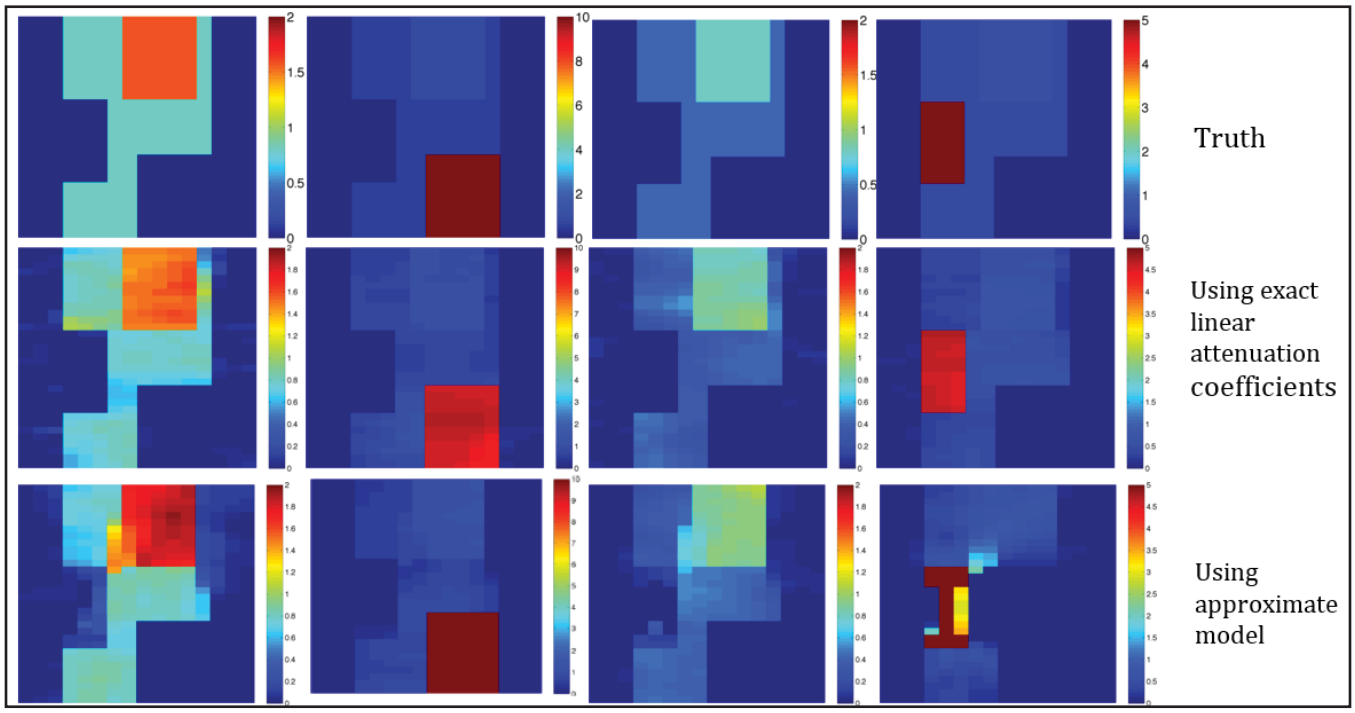

Figure 6: Images of coherent scatter form factors at 0.86, 1.30, 1.66 and 2.14 nm^{-1} using the tomographic imaging architecture of Figure 3.

We performed a similar analysis using the coded aperture architecture of Figure 4 with 3 illumination directions. To simplify the reconstruction, we used monochromatic illumination. The results are shown in Figure 7 (on the next page). Note that the peak corresponding to graphite at 1.3 nm^{-1} has been smeared over a larger area, and the peak corresponding to aluminum at 2.14 nm^{-1} has been eliminated. There are also issues with respect to the form factors for the amorphous materials. The results imply that, for this coded aperture architecture, it is essential to use fusion information regarding linear attenuation coefficients in order to compensate for photon path loss in the reconstruction algorithms. This can be explained in part because the coherent scatter reaching any one detector comes from many different rays, so the approximation using the transmission attenuation is much less accurate than when you restrict scatter to a vertical direction along an incoming ray, which was homogeneous given the vertical symmetry of our phantom object.

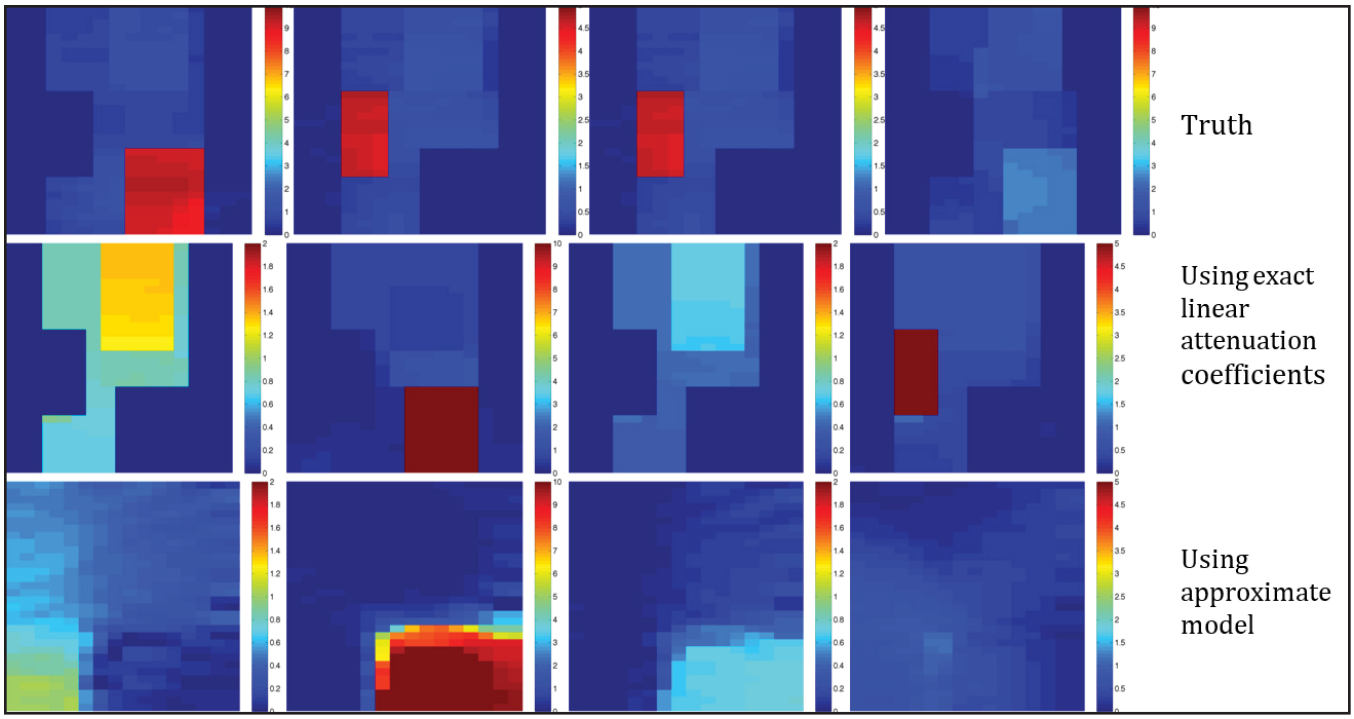

Figure 7: Images of coherent scatter form factors at 0.86, 1.30, 1.66 and 2.14 nm-1 using the coded aperture imaging architecture of Figure 4.

We also conducted experiments to illustrate the performances of the different algorithms. Using the coded aperture architecture with three different illumination directions and photon-counting detectors with 4 keV resolution, we compare the reconstructions obtained by algorithms IRL1, IREP and a variation called IREP-C documented in [25], that uses object boundaries obtained from CT images. The results, shown in Figure 8 (on the next page), indicates that the crystalline regions are reconstructed homogeneously and clearly by the different algorithms. In particular, the IREP algorithms localize the geographic extent of the crystalline regions well, with sharp, accurate boundaries. However, there is reconstruction of the amorphous materials, as energy from the peaks of the crystalline materials appears at other momentum transfer levels. Note also that the IREP and IRL1 algorithms have difficulty segmenting the aluminum block due to significant self-attenuation of the scattered photons in the aluminum block, whereas the IREP-C algorithm has much more accurate reconstruction in that area.

We also developed a new class of algorithms for reconstruction of X-ray diffraction images based on image dictionaries. Our goal was to improve reconstruction of the amorphous form factors, which were difficult to reconstruct in our previous approaches, as indicated by our results in Figures 6-7, and Figure 8 (on the next page). Dictionary-based processing is a recent tool used in image processing for a variety of problems, from denoising to inpainting. In our prior work [16 and 26], we had shown that using known form factors for specific materials as dictionary elements for reconstruction yielded improved accuracy for non-crystalline coherent scatter form factors. However, the set of all possible compounds would yield too large a dictionary for such techniques to be practical.

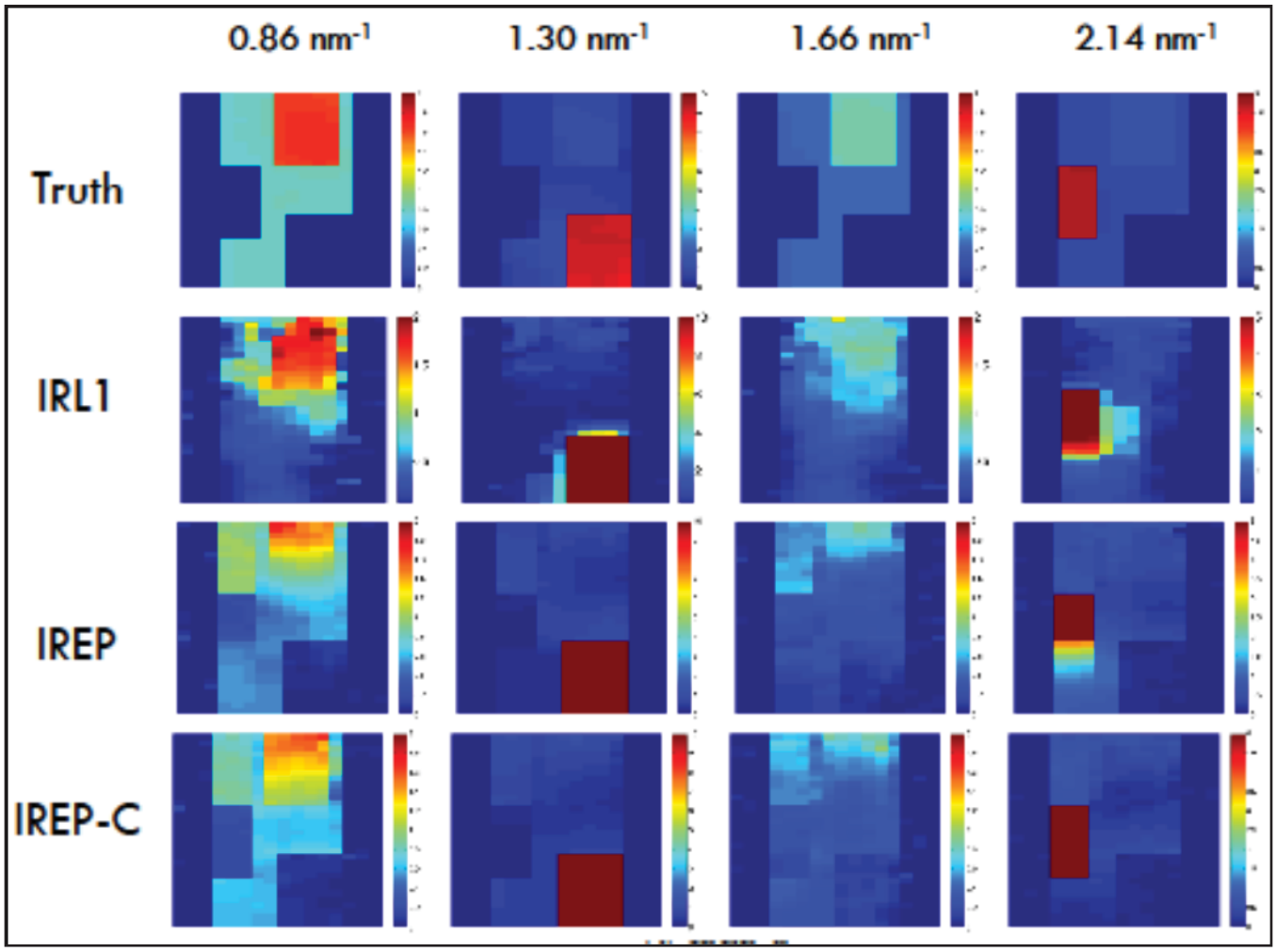

Figure 8: Images of coherent scatter form factors at 0.86, 1.30, 1.66 and 2.14 nm^{-1} obtained for different reconstruction algorithms using the coded aperture imaging architecture of Figure 4.

Instead, we designed an overcomplete dictionary of splines tailored to exploit the coherent scatter form factor structure across the momentum transfer direction with sharp peaks for crystalline materials and smooth variations. The basis functions for this dictionary are shown in Figure 9. We then designed an inverse image formation algorithm that extended our IRL1 algorithm to represent the resulting q-images at each location as a sparse sum of multiples of dictionary elements, exploiting principles of compressive representations by including an l_1 penalty on non-zero coefficients in the objective function. Thus, the objective function included a spatial smoothness objective to represent object regions, and a sparse form factor representation to encourage the use of a small number of basis functions to represent the underlying coherent form factors. We refer to this new algorithm as IRWS.

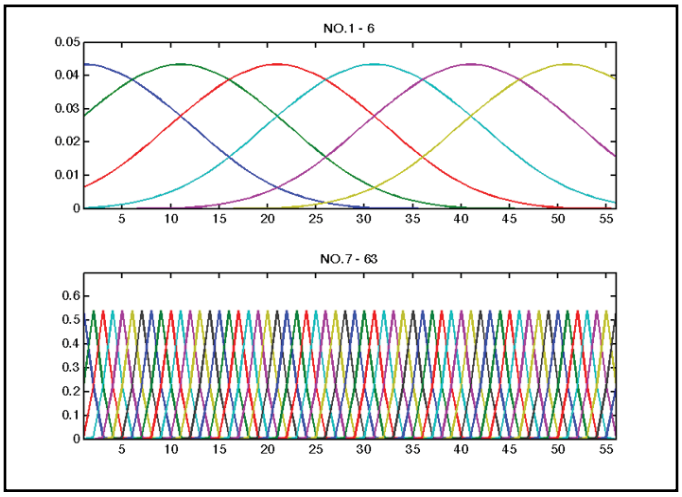

Figure 9: Dictionary of spline functions for fitting sharp peaks and smooth form factors.

The performance for the IRWS reconstructions is shown in Figure 10 for data collected using the coded aperture architecture of Figure 4. The results show improved reconstruction of the areas where non-crystalline materials are present, supporting our conjecture that dictionary representations would be useful. Our final investigation in this project expanded on the idea of dictionary representations. In the past decade, several groups [27 and 28] have proposed techniques for learning dictionary elements and adapting them based on the specific image being processed. These techniques have been used primarily for image enhancement and restoration, not for inverse problems. In the context of image enhancement, the techniques have shown improved design of basis functions that lead to sparse representations and improved image quality. We extended techniques such as K-SVD [27] to apply to dictionary learning for X-ray diffraction imaging. We found there is one significant difference in the tomography problem from the image restoration problem: the observation operator is non-local, which makes learning a dictionary for local patches difficult. In our implementation, we used the IRL1 algorithm to construct an initial X-ray diffraction image, which we used to learn an overcomplete dictionary basis. We found that the quality of reconstruction obtained from the initial IRL1 image was insufficient to identify good dictionary elements in this problem. Given the complexity of this problem, we thought it would be best to focus the use of adaptive dictionary learning on simpler problems such as artifact mitigation in conventional CT.

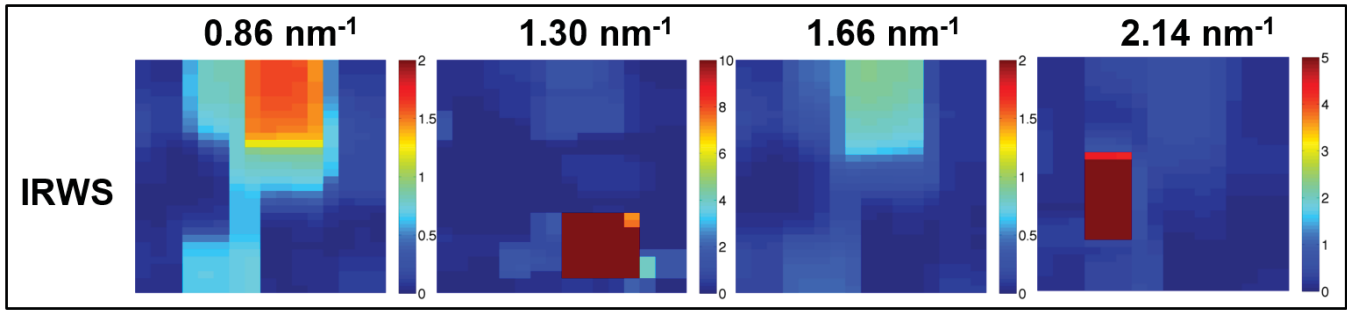

Figure 10: Images of coherent scatter form factors at 0.86, 1.30, 1.66 and 2.14 nm^{-1} obtained for IRWS algorithm using the coded aperture imaging architecture of Figure 4.

Our results established the feasibility of new classes of X-ray diffraction imaging architectures based on tomographic principles with sparse observation geometries that increase the amount of observed scattered radiation versus current approaches, and which can generate X-ray diffraction images in a timely manner. Our results also identified the need for including energy-sensitive detectors as well as the integration of information from dual-energy CT systems in order to properly reconstruct the diffraction images using advanced computational imaging techniques. Our investigations also established the presence of potential new classes of artifacts that result from inclusion of metallic materials with high linear attenuation along with softer materials such as liquids, plastics, and organic materials. These artifacts include spectral contamination where crystalline peaks in the form factors from one material appears in nearby materials, to obscuration due to attenuation of the scattered spectra and increased noise due to lack of collimation to reduce incoherent scatter. These pose significant challenges that must be addressed through the use of advanced algorithms such as the ones developed in this work.

There are several directions in which this work could be extended, including further experimentation with different materials, development of faster reconstruction algorithms, and evaluating different architectures. However, there is much work in industry that is currently considering the development of new architectures for XDI. The extensions of this work need to wait for further architecture definition by the DHS vendor community so as to be relevant for the emerging new devices. Our current results are sufficient to provide support in these architecture design endeavors.

D. Major Contributions

The above outcomes were accomplished by Year 2:

- Provided a systematic analysis of alternative X-ray diffraction architectures and established performance limitations as well as requirements for fusion with dual-energy CT.
- Developed advanced algorithms for tomographic reconstruction of X-ray diffraction images and characterized their relative performance.
- Developed results that establish the feasibility of tomographic X-ray diffraction architectures that have greater efficiency in collecting coherent scatter signals when compared with current commercial models.
- Developed extensions to advanced image processing techniques such as dictionary-based image enhancement to apply to X-ray diffraction imaging and evaluated the performance of these extensions.

In Year 3, the only outcome was:

- Transfer of algorithm software and data sets for exploration in multi-energy CT reconstruction and in analysis of performance for alternative checked luggage imaging systems.

E. Milestones

The only milestone in Year 3 Work Plan was:

- Transfer of algorithm software and data sets for exploration in multi-energy CT reconstruction and in analysis of performance for alternative checked luggage imaging systems.

This milestone was achieved in Year 3.

F. Future Plans

As indicated, this project has achieved its milestones and will not continue as part of the ALERT research portfolio. The student involved in the project will be focusing on a new direction involving adaptive reconstruction for artifact mitigation in CT imagery motivated by check point and checked luggage dual-energy CT, which is ALERT project R4-C.1. We will transition the work in this project to support our effort under DHS BAA 13-05 that includes analysis of multi-modal object recognition with new signatures such as X-ray form factors of materials.

III. RELEVANCE AND TRANSITION

A. Relevance of Research to the DHS Enterprise

This project is developing technologies for improving automated detection and classification of explosive materials in checked luggage by imaging additional properties of materials that can provide improved discriminants. Of particular interest is the potential for improving detection of complex explosives such as liquids and homemade explosives (HMEs) using these advanced discriminants.

B. Potential for Transition

Prototype X-ray diffraction systems are currently under investigation or development by many companies, including Morpho, Analogic, L-3, Reveal and others. We have presented our results to each of these groups to integrate into their design considerations.

C. Data and/or IP Acquisition Strategy

We have no plans to acquire further data at this point. There are no systems currently built that work on tomographic principles, so data has to be simulated. In terms of IP, all of our results are available in the public domain.

D. Transition Pathway

We have presented our investigations and discussed the results with several potential end users. They will integrate the lessons learned into their development process. If there is opportunity for specific algorithm technology that is well-suited for their use, we will assist in transitioning that technology and tailoring it for their specific system design.

E. Customer Connections

- David Lieblich, Analogic (infrequent seminar and discussions) – interested in results, but not involved in project.
- Boris Oreper and David Perticone, L-3 Communications (infrequent seminar, discussions) – interested in results, but not involved in project.
- Robert Shuchatowitz, Reveal Imaging (infrequent seminar, discussions) – interested in results, but not involved in project.
- Sondre Skatter and Matthew Merzbacher, Morpho Detection – (technical discussions) – interested in results, but not involved in project.

IV. REFERENCES

[1] Weisenseel, R.A., Karl, W.C., and Chan, R., "Shared-boundary fusion for estimation of noisy multi-modality atherosclerotic plaque imagery," Proc. 2002 IEEE International Conference on Image Processing, Rochester, NY, pp. 157-160, Sep. 2002.

[2] Weisenseel, R., Karl, W.C., Chan, R.C., and Brady, T.J., "A Variational Approach to Multi-modality Subsurface Data Inversion and Fusion Based on Shared Image Structure," Subsurface Sensing Technologies and Applications, vol. 4, no. 4, pp. 373-392, Oct. 2003.

[3] Weisenseel, R.A., Chan, R.C., and Karl, W.C., "Multi-Sensor Data Inversion and Fusion Based on Shared Image Structure," Multi-sensor Image Fusion and Its Applications, Eds: R. Blum and Z. Liu. CRC Press, 2005.

[4] K. Chen and D. Castañón, "Robust Multifrequency Inversion in Terahertz Diffraction Tomography," Proc. IS&T/SPIE Electronic Imaging, January 2011, San Francisco, CA.

[5] G. Harding, H. Strecker, S. Olesinski, and K Frutschy, "Radiation source considerations relevant to next-generation X-ray diffraction imaging for security screening applications", Proc. SPIE, Vol. 7450, 2009.

[6] U. van Stevendaal, J.-P. Schlomka, A. Harding, and M. Grass., "A reconstruction algorithm for coherent scatter computed tomography based on filtered back-projection", Med. Phys., 30(9), pp. 2465—2474, 2003.

[7] S. M. Schneider, J. Schlomka, and G. L. Harding., "Coherent Scatter Computed Tomography Applying a Fan-Beam Geometry", Proc. SPIE, Vol. 4320, pp. 754—763, 2001.

[8] Harding, G. and Harding, A., [Counterterrorist detection techniques of explosives], ch. 8, Elsevier (2007).

[9] Harding, G., "X-ray diffraction imaging - a multi-generational perspective," Applied Radiation and Isotopes 67, 287-295 (2009).
[10] Harding, G., Strecker, H., Kosciesza, D., and Gordon, J., "Detector considerations relevant to X-ray diffraction imaging for security screening application," Proceedings of SPIE 7306, 730619-1-730619-11 (2009).
[11] Harding, G., Kosanetzky, J., and Neitzel, U., "X-ray diffraction computed tomography," Medical Physics 14(4) (1987).
[12] Harding, G. and Kosanetzky, J., "Status and outlook of coherent-X-ray scatter imaging," J. Opt. Soc. Am. A 4(5), 933-944 (1987).
[13] Grant, J. A., Morgan, M. J., Davis, J. R., and Wells, P., "Reconstruction strategy suited to X-ray diffraction tomography," J. Opt. Soc. Am. A 12(2), 291-300 (1995).
[14] Schneider, S. M., Schlomka, J., and Harding, G., "Coherent scatter computed tomography applying a fan-beam geometry," Proceedings of SPIE 4320, 754-630 (2001).
[15] Stevendaal, U. V., Schlomka, J., Harding, A., and Grass, M., "A reconstruction algorithm for coherent scatter computed tomography based on filtered back-projection," Medical Physics 30(9), 2465-2474 (2003).
[16] K. Chen and D. Castañón, " A regularized iterative reconstruction algorithm for X-ray diffraction tomography," Proc. SPIE Conf. on Defense, Security and Sensing, 83740D, Baltimore, MD, April 2012.
[17] K. Chen and D. Castañón, " Algorithms and Architectures for X-ray diffraction tomography," Computational Imaging, C. A. Bouman, K. Sauer, eds, Proc. SPIE, Vol. 9020, San Francisco, CA Feb. 2014.
[18] K. MacCabe, K. Krishnamurthy, A. Chawla, D. Marks, E. Samei, and D. Brady, "Pencil beam coded aperture x-ray scatter imaging," Optics Express, Vol. 20, Issue 15, 2012.
[19] K. P. MacCabe, A. D. Holmgren, J. A. Greenberg, and D. J. Brady, "Coding for x-ray scatter imaging," Imaging and Applied Optics, June 2013.
[20] A. J. Kapadia, M. N. Lakshmana, K. Krishnamurthy. P. Sahbaee, A. Chawla, S. Wolter, K. MacCabe, D. Brady and E. Samei, "Monte-Carlo simulations of a coded-aperture x-ray scatter imaging system for molecular imaging," Proc. SPIE 8668, Medical Imaging 2013: Physics of Medical Imaging, March, 2013.
[21] Analyst. 2014 Feb 21; 139(4):709-13. doi: 10.1039/c3an01641b.
[22] J. A. Greenberg, M. Hassan, K. Krishnamurthy and D. Brady, "Structured illumination for tomographic X-ray diffraction imaging," Analyst. 2014 Feb 21;139(4):709-13
[23] S. Pang, M. Hassan, J. Greenberg, A. Holmgren, K. Krishnamurthy and D. Brady, "Complementary coded apertures for 4-dimensional x-ray coherent scatter imaging," Optics Express, 2014.
[24] J. Greenberg, K. Krishnamurthy, M. Lakshmanan, K. MacCabe, S. Wolter, A. Kapadia, and D. Brady, "Coding and sampling for compressive X-ray tomography," Proceedings of SPIE, 2013.
[25] S. Agostinelli et al., "Geant4—a simulation toolkit," Nuclear Instruments and Methods in Physics Research, Vol. 506, July 2003.
[26] K. Chen, Reconstruction algorithms for multispecgral diffraction imaging, Dept. of Electrical Engineering, Boston University, May 2014.
[27] M. Aharon, M. Elad, and Alfred Bruckstein, "K-SVD: An algorithm for designing overcomplete dictionaries for sparse representation", IEEE Transactions on Signal Processing, Vol. 54, No. 11, 2006.
[28] J. Mairai, F. Bach, J. Ponce and G. Sapiro, "Online dictionary learning for sparse coding," Proc. Intnl. Conf. on Machine Learning, Montreal, CA June, 2009.